Hydrogenation induced carrier mobility polarity reversal in single layer AlN

Hydrogenation induced carrier mobility polarity reversal in single layer AlN

Lijia Tong[1], Zheng Chen[1,a)], Bin Wang[2], Hongxiang Zong[3,4,b)] and Graeme J. Ackland[4]

[1]*State Key Laboratory of Solidification Processing, School of Materials Science and Engineering, Northwestern Polytechnical University, Xi'an 710072, PR China*

[2]*Department of Physics, Shenzhen University, Shenzhen, Guangdong 518060, PR China*

[3]*State Key Laboratory for Mechanical Behavior of Materials, Xi'an Jiaotong University, Xi'an 710049, PR China*

[4]*Centre for Science at Extreme Conditions (CSEC), School of Physics and Astronomy, University of Edinburgh, Edinburgh EH9 3FD, UK*

Two-dimensional (2D) materials promote the development of nanoelectronic devices, which requires candidate systems with both a high carrier mobility and a sufficiently large electronic bandgap. We present a first principles calculation of the intrinsic carrier mobilities of pristine (1L-AlN) and hydrogenated (1L-AlN-H_2) AlN nanosheets. Numerical results show that 1L-AlN shows a hole-dominated ultra-large carrier mobility (up to 3000 $cm^2V^{-1}s^{-1}$). Upon fully-hydrogenation (1L-AlN-H_2), the polarity of carrier mobility is reversed from hole-dominated to electron-dominated. This tunable polarity of intrinsic carrier mobility indicates single layer AlN nanosheet a promising candidate for future nano-electronics.

High carrier mobility and moderate band gap are two most important factors of fabricating high-performance nanoelectronic devices. The former ensures efficient manipulation of charge carriers, and the later indicates the capability of controlling the charge carriers by the external electric field[1]. Graphene and MoS_2 are two of the most important two-dimensional (2D) materials, which are extensively considered as good candidates of low dimensional nanoelectronic devices. However, the band gap of graphene is almost equal to zero although its mobility is ultra-high[2]. 2D MoS_2 has finite band gap, but its carrier mobility is relatively low （$60\sim200$ $cm^2V^{-1}s^{-1}$） which is roughly one order smaller than that of conventional silicon-based semiconductors (~500 $cm^2V^{-1}s^{-1}$)[3]. It is necessary and significant to explore a potential 2D material for assembling robust nanoelectronics devices, which has not only high carrier mobility but also controlling finite band gap.

Among the potential two-dimensional (2D) materials, single layer AlN (1L-AlN) is currently an object of much interest due to its semiconducting nature and its large band gap[4, 5]. Recently, ultrathin (sub-monolayer to 12 monolayers) graphene-like hexagonal AlN has been realized experimentally by Tsipas *et al.*[6]. They reported that these ultrathin AlN nanosheets display good quality epitaxial growth characteristics and minimal residual oxygen incorporation on the surface. Motivated by this report, Bacaksiz *et al.* investigated the frontier orbitals of 1L-AlN[4]. They predicted that the valence band maximum (VBM) of 1L-AlN is mainly composed of out-plane N-p_z orbitals[4], which may ultimately result in a high hole carrier mobility. In addition, fully-functionalization can saturate the N-p_z orbitals and induce pucker of single layer AlN[7, 8], which may play an important role in modulating the carrier mobility of monolayer AlN.

Previous investigations indicated that the coherent wavelength of thermally activated carriers at room temperature is much larger than the bond length and is very close to the acoustic phonon wavelength in inorganic semiconductors[9-11]. Thus, the scattering at low energy regime

a) Electronic addresses: chenzh@nwpu.edu.cn
b) Electronic addresses: zonghust@mail.xjtu.edu.cn

is mostly dominated by the electron-acoustic phonon coupling [12, 13]. According to the arguments proposed by Bardeen and Shockley[14-16], the scattering due to the electron-acoustic phonon coupling can be described effectively by the deformation potential (DP) theory. Within the effective mass approximation, the DP theory can be effectively applied to the two-dimensional (2D) materials and the carrier mobility μ_{2D} can be calculated by

$$\mu_{2D} = \frac{2e\hbar^3 C^{2D}}{3k_B T \left|m^*\right|^2 E_1^{\,2}}, \qquad (1)$$

where $m^* = \hbar[\partial^2 E(k)/\partial^2 k]^{-1}$ is the effective mass and T is the temperature. E_1 represents the deformation potential constant of the valence-band minimum (VBM) for hole or conduction-band maximum (CBM) for electron along the transport direction, which is defined as $E_1 = \mathrm{d}E_{edge}/\mathrm{d}\delta$ with E_{edge} the energy of CBM\VBM under proper cell compression and $\mathrm{d}\delta$ the infinitesimal of structure deformation. C^{2D} is the in-plane elastic modulus and is defined as $C^{2D} = [\partial^2 E/\partial\delta^2]/S_0$, where E is the total energy of the supercell, δ is the applied uniaxial strain and S_0 is the area of the supercell.

In the present work, we carried out first principles calculation using Vienna Ab-initio Simulation Package (VASP) to investigate the carrier mobilities of 1L-AlN and fully-hydrogenated 1L-AlN using Eq. (1). Numerical calculation is performed by using the projector augmented wave method with the Perdew-Burke-Ernzerhof functional (PAW-PBE), which has been extensively employed to study the geometric and electronic properties of AlN nanostructures[4, 5, 7, 8, 17, 18]. The energy cutoff for the plane-wave basis was set to 500 eV for all calculations. Numerical results show that the carrier mobility of 1L-AlN at room temperature is relatively high, which is up to ~3000 $cm^2V^{-1}s^{-1}$ and is hole-dominated. While for the fully-hydrogenated 1L-AlN (1L-AlN-H_2), the carrier mobility is largely decreased and changes from holes-dominated to electrons-dominated. This behavior indicates that the 1L-AlN can be assembled to conductivity-adjustable nanoelectronics device by hydrogen saturation. The detailed analysis is shown as follows.

Firstly, we investigated the electronic structure and acoustic phonon-limited mobility of 1L-AlN. In order to intuitively demonstrate the carrier conduction along the zigzag and armchair directions, an orthogonal supercell is used. The corresponding atomic structure is shown in Fig. 1a, where the orthogonal super cell vectors $\mathbf{a_{ox}} = a(1, 0, 0)$ and $\mathbf{a_{oy}} = a(0, \sqrt{3}, 0)$ (the lattice constant a = 3.13 Å) are signified with red arrows, together with the hexagonal primitive cell vectors $\mathbf{a_{hx}} = a(1, 0, 0)$ and $\mathbf{a_{hy}} = a(0.5, \sqrt{3}/2, 0)$ with black arrows for comparison. The right panel of Fig. 1a shows the first Brillouin zone (FBZ) and Fig. 1b shows the band structure of 1L-AlN. The K point (fractional reciprocal coordinates: 1/3, 2/3, unit is 2π/a) defined in reciprocal lattice of the primitive cell is folded into (1/3, 0) point sitting at the Γ-X branch in the FBZ of the orthogonal supercell (see Fig. 1a).

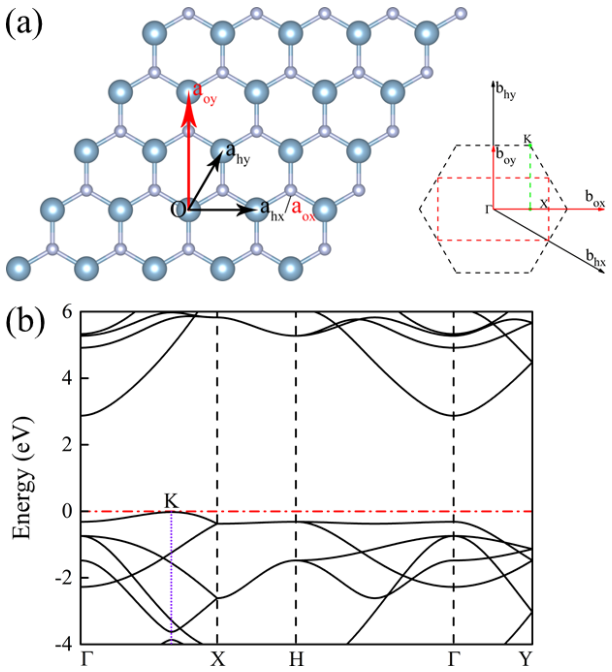

FIG. 1. Atomic structure model and band structure of single layer AlN (1L-AlN). (a) Left panel: structural schematic diagram of 1L-AlN. The black and red arrow lines represent the hexagonal unit vectors ($\mathbf{a}_{ox}$ and $\mathbf{a}_{oy}$) and the orthogonal supercell vectors ($\mathbf{a}_{hx}$ and $\mathbf{a}_{hy}$), respectively. Right panel: the first Brillouin zone (FBZ) associated with two sets of k vectors. $\mathbf{B_{ox}}$ and $\mathbf{b_{ox}}$ are the k vector of hexagonal primitive cell. $\mathbf{B_{hx}}$ and $\mathbf{b_{hx}}$ are the k vector of orthogonal super cell. The green dashed line shows the folding of the K point from the FBZ of the hexagonal lattice to the FBZ of the orthogonal lattice. (b) Band structure of 1L-AlN (the orthogonal supercell). The large balls indicate the Al atoms and the small balls indicate the N atoms.

As described in Eq. (1), the carrier mobility of 2D materials is determined by m^*, C^{2D} and E_1, so all these quantities are calculated firstly from first principles and the corresponding values are listed in Table 1. The effective mass $m^*_{\alpha\beta}$ tensor is calculated by $\hbar^2[\partial^2\varepsilon(k)/\partial k_\alpha \partial k_\beta]^{-1}$ along $\mathbf{a_{ox}}$ and $\mathbf{a_{oy}}$ directions, respectively, which indeed reveals a different value for holes

(1.33m_e along $\mathbf{a_{ox}}$ direction and 1.52m_e along $\mathbf{a_{oy}}$ direction) and an equal value for electrons (0.51m_e along both $\mathbf{a_{ox}}$ and $\mathbf{a_{oy}}$ directions). While, for C^{2D} and E_1, the values are very close along $\mathbf{a_{ox}}$ and $\mathbf{a_{oy}}$ directions for both electrons and holes.

As a result, the acoustic phonon-limited mobilities μ at room temperature (300 K) were calculated according to Eq. (1). As shown in Table 1, the electron mobility is 300.92 along zigzag direction ($\mathbf{a_{ox}}$ direction) and 298.33 $cm^2V^{-1}s^{-1}$ along armchair direction ($\mathbf{a_{oy}}$ direction), respectively. It is significantly larger than the electron mobility of single layer MoS_2 (60~72 $cm^2V^{-1}s^{-1}$)[9, 10]. Simultaneously, we found that the hole mobilities (2795~3701 $cm^2V^{-1}s^{-1}$) is much higher than the electron mobility (almost 9~12 times), which is even higher than that of typical silicon-based devices (~500 $cm^2V^{-1}s^{-1}$)[3]. This strong electron/hole mobility polarization originates from a sharp difference (almost 9 times) of $|E_1|$ between hole and electron, which will be discussed later.

TABLE I. Predicated Carrier Mobility in AlN nanosheets[a].

	type	m^*	E_1	C^{2D}	μ
1L-AlN	e (a_{ox})	0.51	-5.08	143.89	300.92
	e (a_{oy})	0.51	-5.08	143.75	298.33
	h (a_{ox})	1.33	-0.55	143.89	3700.96
	h (a_{oy})	1.52	-0.56	143.75	2795.66
1L-AlN-H_2	e (a_{ox})	0.80	-2.38	84.40	326.24
	e (a_{oy})	0.80	-2.38	84.30	327.18
	h (a_{ox})	1.84	-2.94	84.40	40.20
	h (a_{oy})	1.91	-2.94	84.30	37.51

[a]"1L-AlN" and "1L-AlN-H2" represent pristine and fully-hydrogenated AlN nanosheet, respectively. Types "e" and "h" denote the "electron" and "hole", respectively. m^* (in unit of m_e) represents the effective mass. E_1 (in units of electronvolts) is the deformation potential. C^{2D} is the 2D elastic modulus, which is in units of N/m. Carrier mobility μ (in units of $cm^2V^{-1}s^{-1}$) is calculated using Equation (1) with temperature T = 300 K.

In the following, we investigate the carrier mobility of 1L-AlN-H_2 and analyze the influence of fully-functionalization to the carrier mobility. The orthogonal super cell of 1L-AlN-H_2 resembles that of 1L-AlN except a litter larger lattice constant a (a = 3.14 Å). The corresponding geometric structure and band structure of 1L-AlN-H_2 are shown in Fig. 2. Different from the pristine ones, the hydrogenated AlN nanosheet possesses a quasi-bulk-like wurtzite structure with a bandgap of 3.01 eV. Based on the band structure, the quantities m^*, C^{2D}, E_1 and finally μ were all calculated and listed in Table 1. Numerical results show that the effective masses m^* of 1L-AlN-H_2 is larger than 1L-AlN for both electrons and holes along zigzag and armchair directions. In contrast, C^{2D} decreases after fully hydrogenation as a result of the change from sp^2 orbitals (1L-AlN) to tetrahedrally coordinated sp^3 orbitals (1L-AlN-H_2)[19]. Different from the monotone change of C^{2D} and m^*, E_1 show a diverse trend upon fully-hydrogenation, where the hole $|E_1|$ increase upon fully-hydrogenation and electron $|E_1|$ decrease upon fully-hydrogenation. Finally, the carrier mobility μ of electrons and holes of 1L-AlN-H_2 show different behaviors to the hydrogenation. The electron mobility remains the same level as that of 1L-AlN along both zigzag and armchair direction, which indicate week relevance between hydrogenation and electron mobility. While, the hole mobility plunges from roughly 3000 $cm^2V^{-1}s^{-1}$ to ~40 $cm^2V^{-1}s^{-1}$ for both directions due to the suddenly increase of hole $|E_1|$ after the hydrogenation. As a result, the hole dominated carrier mobility of 1L-AlN is changed to the electron dominated carrier mobility of 1L-AlN-H_2, which means a reversal of intrinsic carrier mobility polarity can be achieved via fully-hydrogenation.

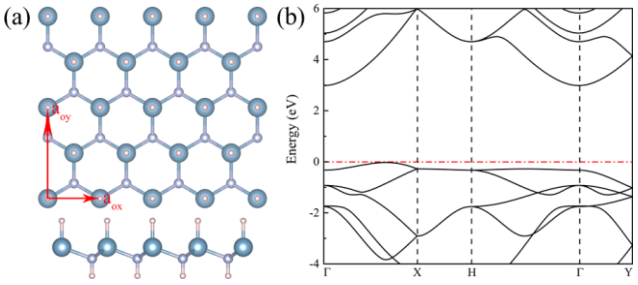

FIG. 2. Lattice and electronic structures of orthogonal monolayer hydrogenated single layer AlN (1L-AlN-H_2). (a) Atomic structure of 1L-AlN-H_2 (top and side views) with lattice vectors ($\mathbf{a_{ox}}$ and $\mathbf{a_{oy}}$). (c) Electronic band structures for 1L-AlN-H_2.

Combining Eq.(1) and the data in Table 1, we concluded that $|E_1|$ plays an important role to the polarity-reversion of μ after the fully hydrogenation of 1L-AlN. The deformation of potential constant E_1 can be understood by analyzing the wavefunction distribution of CBM and VBM before and after the hydrogenation[9, 11, 20, 21].

Fig.3 shows the real space distributions of CBM and VBM of 1L-AlN and 1L-AlN-H_2, respectively. We firstly analyze the CBM and VBM of 1L-AlN. The CBM of 1L-AlN is composed of the in-plane part and out-plane part as shown in Fig.3(a). The out-plane wavefunction is robust to in-plane strain and contributes a small E_1[9, 11, 20]. By contrast, the in-

plane wavefunction mainly consists of *s* orbitals of N atoms (N-*s*) as shown in Fig. 3a, which are sensitive to in-plane strain and induces a large electron $|E_1|$ equal to 5.08 eV. While, the VBM of 1L-AlN mainly stems from p_z orbitals of N atoms which are perpendicular to the 2D plane of 1L-AlN as shown in Fig. 3b. The N-p_z orbitals make little change as the in-plane strain, resulting a very small hole $|E_1|$ roughly equal to 0.55 eV. The combination of in-plane N-*s* orbitals associated with CBM and out-plane N-p_z orbitals associated with VBM lead to the electron dominated polarity for 1L-AlN.

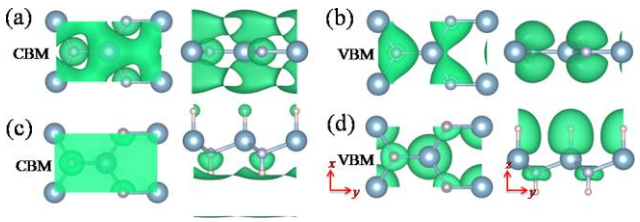

FIG. 3. The band decomposed charge densities of conduction band bottom (CBM) and valence band maximum (VBM). (a, b) for 1L-AlN. (c, d) for 1L-AlN-H_2. The isosurface level is set at 0.02 e/Å^3. The big, middle and small balls represent Al, N and H atoms, respectively.

Then we analyze the CBM and VBM of 1L-AlN-H_2. Similar to 1L-AlN, the CBM of 1L-AlN-H_2 also comprises crucial in-plane part and negligible out-plane part as shown in Fig. 3c. However, the in-plane part of 1L-AlN-H_2 only consists of partial N-*s* orbitals different from that of 1L-AlN which consists of integral N-*s* orbitals (see the difference between Fig. 3a and Fig. 3c). As a result, few N-*s* orbitals of 1L-AlN-H_2 contribute a smaller electron $|E_1|$ compared to 1L-AlN as indicated in Table 1. While, for the VBM of 1L-AlN-H_2, although it mainly derive from *s* orbitals of H atoms (H-s) as shown in Fig. 3b[22], the out-plane H-*s* orbitals are not vulnerable to in-plane strain[9, 11, 20]. Further analysis shows that the largely increased hole $|E_1|$ (2.94 eV) of 1L-AlN-H_2 compared to that of 1L-AlN comes from the in-plane N-p_xp_y orbitals as shown in Fig. 3b. The in-plane N-p_xp_y orbitals are more susceptible to in-plane strain than the partial N-*s* orbitals[9, 11, 20], which ultimately induces a larger hole $|E_1|$ (2.94 eV) than electron $|E_1|$ (2.38 eV) in 1L-AlN-H_2 and polarity-reversed carrier mobility compared to 1L-AlN[9].

In conclusion, we have investigated the carrier mobilities of 1L-AlN and 1L-AlN-H_2 using first principles calculation. Numerical results show that monolayer AlN has lager and tunable carrier mobility. The carrier mobility of 1L-AlN is hole-dominated, while the carrier mobility of 1L-AlN-H_2 is electron-dominated, which indicates the polarity of carrier mobility can be adjusted and reversed by hydrogenation.

Project supported by the National Natural Science Foundation of China (51674205, 51474176, 51475378, 51575452), the Natural Science Basic Research Plan in Shaanxi Province of China (2016JQ5014). We would like to thank the National Supercomputer in GuanZhou for computational facilities.

[1]C. Sun, H. Xiang, B. Xu, Y. Xia, J. Yin, and Z. Liu, Applied Physics Express **9**, 035203 (2016).
[2]A. C. Ferrari, et al., Nanoscale **7**, 4598 (2015).
[3]L. Li, Y. Yu, G. J. Ye, Q. Ge, X. Ou, H. Wu, D. Feng, X. H. Chen, and Y. Zhang, Nature nanotechnology **9**, 372 (2014).
[4]C. Bacaksiz, H. Sahin, H. D. Ozaydin, S. Horzum, R. T. Senger, and F. M. Peeters, Physical Review B **91** (2015).
[5]Y. Peng, C. Xia, H. Zhang, T. Wang, S. Wei, and Y. Jia, Journal of Applied Physics **116**, 044306 (2014).
[6]P. Tsipas, et al., Applied Physics Letters **103**, 251605 (2013).
[7]W. X. Zhang, T. Li, S. B. Gong, C. He, and L. Duan, Physical chemistry chemical physics : PCCP **17**, 10919 (2015).
[8]Y. Wang and S. Shi, Solid State Communications **150**, 1473 (2010).
[9]Y. Cai, G. Zhang, and Y. W. Zhang, Journal of the American Chemical Society **136**, 6269 (2014).
[10]Jin Xiao, Mengqiu Long, MingJun Li, Xinmei Li, Hui Xu, and K. Chan, Physical chemistry chemical physics : PCCP **17**, 9 (2015).
[11]J. Qiao, X. Kong, Z. X. Hu, F. Yang, and W. Ji, Nature communications **5**, 4475 (2014).
[12]K. Kaasbjerg, K. S. Thygesen, and K. W. Jacobsen, Physical Review B **85** (2012).
[13]K. Kaasbjerg, K. S. Thygesen, and A.-P. Jauho, Physical Review B **87** (2013).
[14]J. Bardeen and W. Shockley, Physical Review **80**, 72 (1950).
[15]B. Xu, Y. D. Xia, J. Yin, X. G. Wan, K. Jiang, A. D. Li, D. Wu, and Z. G. Liu, Applied Physics Letters **96**, 183108 (2010).
[16]S. Bruzzone and G. Fiori, Applied Physics Letters **99**, 222108 (2011).
[17]L. Tong, Z. Chen, H. Zong, L. Huang, R. Bai, and J. Zhang, physica status solidi (b) **253**, 1643 (2016).
[18]L. Tong, Z. Chen, J. Li, H. Zong, and J. Zhang, physica status solidi (b) **254**, 1600489 (2017).
[19]H. Şahin, S. Cahangirov, M. Topsakal, E. Bekaroglu, E. Akturk, R. T. Senger, and S. Ciraci, Physical Review B **80** (2009).
[20]M. Q. Long, L. Tang, D. Wang, L. Wang, and Z. Shuai, Journal of the American Chemical Society **131**, 17728 (2009).
[21]M. Long, L. Tang, D. Wang, Y. Li, and Z. Shuai, ACS Nano **5**, 2593 (2011).
[22]C. W. Zhang and F. B. Zheng, J Comput Chem **32**, 3122 (2011).